Characterization of the histone methyltransferase PRDM9 using biochemical, biophysical and chemical biology techniques

Article (Accepted Version)

Characterization of the Histone Methyltransferase PRDM9 Utilizing Biochemical, Biophysical and Chemical Biology Techniques*

Xiaoying Koh-Stenta[1], Joma Joy[1], Anders Poulsen[1], Rong Li[1], Yvonne Tan[1], Jung-Hyun Min[3], Liling Wu[2], Anna Ngo[1], Jianhe Peng[1], Wei Guang Seetoh[1], Jing Cao[1], John Liang Kuan Wee[1], Perlyn Zekui Kwek[1], Alvin Hung[1], Umayal Lakshmanan[1], Horst Flotow[1], Ernesto Guccione[2], and Jeffrey Hill[1]

From the [1]Experimental Therapeutics Centre, and the [2]Institute for Molecular and Cell Biology, Agency for Science, Technology and Research (A*STAR), Singapore 138669, Singapore

[3]Department of Chemistry, University of Illinois at Chicago, Chicago, IL 60607, USA

*Running title: Characterization of the histone methyltransferase PRDM9

To whom correspondence should be addressed: Jeffrey Hill, Experimental Therapeutics Centre, A*STAR, 31 Biopolis Way, Nanos 03-01, Singapore 138669, Tel.: +65 6407-0335; Fax: +65 6478-8768; Email: jhill@etc.a-star.edu.sg

Keywords: PRDM9; histone methyltransferase; biochemical characterization; chemical biology; epigenetics

Background: PRDM family proteins are emerging as an attractive class of epigenetic drug discovery targets.
Results: The histone methyltransferase PRDM9 shows broader activities than previously recognized.
Conclusion: PRDM9 is an archetypal member of the PRDM family with demonstrated chemical tractability.
Significance: This work will facilitate the generation of small drug-like molecules/chemical biology probes for the PRDM family.

ABSTRACT

PRDM proteins have emerged as important regulators of disease and developmental processes. To gain insight into the mechanistic actions of the PRDM family, we have performed a comprehensive characterization of a prototype member protein, the histone methyltransferase PRDM9, utilizing biochemical, biophysical and chemical biology techniques. We report the first known molecular characterization of PRDM9-methylated recombinant histone octamer and the identification of new histone substrates for the enzyme. A single Cys321Pro mutant of the PR/SET domain was demonstrated to significantly weaken PRDM9 activity. Additionally, we have optimized a robust biochemical assay amenable to high throughput screening to facilitate the generation of small molecule chemical probes for this protein family. This work has provided valuable insight into the enzymology of an intrinsically active PRDM protein.

In recent years, the PRDM family of proteins has emerged as a class of putative transcriptional regulators fundamental to the control of cellular differentiation and disease progression. Members of the PRDM family are characterized by a conserved N-terminal PR (PRDI-BF1 and RIZ1 homologous) domain followed by a variable number of zinc-finger repeats. While the PR domain is related to the catalytic SET (Suppressor of variegation 3-9, Enhancer of zeste and Trithorax) domain of a large group of histone lysine methyltransferases, the action of PRDM proteins can either be mediated through recruitment of histone-modifying enzymes (e.g. PRDM1 and -6), or through direct histone lysine methylation (e.g. PRDM2, -8 and -9) (1-8). Deregulation of PRDM expression has been associated with several forms of malignant neoplasia, including leukemia, breast cancer, and gastric cancer (7,9,10). In addition, a growing body of research has demonstrated that

many PRDM proteins are critical for directing a broad range of developmental processes, from primordial germ cell specification to brown fat differentiation (8).

To gain insight into the mechanistic action of this family of proteins, we have selected PRDM9 as a prototype enzyme for comprehensive characterization utilizing biochemical and biophysical approaches. One of seventeen members of the family, the histone methyltransferase PRDM9 was initially identified as Meisetz (meiosis-induced factor containing a PR/SET domain and zinc-finger motif), after the discovery of its role in controlling epigenetic events required for correct meiotic progression (5). Disruption of the *PRDM9* gene in mice results in reduced double-strand break repair, impaired gonad formation, and sterility (5). Subsequent studies have shown that PRDM9 is responsible for zinc-finger binding of specific DNA sequences before crossover, thus providing a molecular basis for recombination hotspot localization (11,12). More recently, meta-analysis of clinical data sets from a range of tumors identified *PRDM9* as a cancer-specific biomarker gene (13). Intrinsic methyltransferase activity of recombinant PRDM9 on histone H3 has been demonstrated and described in the literature (5,6). In addition, a crystal structure of mouse PRDM9 in complex with a histone peptide and *S*-adenosylhomocysteine (SAH) is available (6). The availability of these resources presents a unique opportunity to deepen our understanding of the structural features governing PRDM9 activity.

The data we have generated shows that PRDM9 has the potential to exhibit broad histone substrate recognition extending to all four individual histone core proteins, as well as histone octamers – the basic building blocks of chromatin. Using a robust biochemical assay, we have accomplished the first documented characterization of methyltransferase activity on recombinant histone octamer substrates prepared by co-expressing all four core histones (H2A, H2B, H3 and H4) from a single polycistronic vector (14). A regulatory mechanism of PRDM9 enzymatic activity involving structural rearrangement of substrate and *S*-adenosylmethionine (SAM) binding sites has previously been described (6). Using a combination of biophysical techniques, we tested this hypothesis and demonstrated evidence in support of it. Significantly, growing knowledge about the biological importance and disease relevance of the PRDM family of proteins has brought to the fore their potential as novel targets in epigenetic drug discovery (8,15,16). We have optimized a robust bioluminescent methyltransferase assay amenable to high throughput screening, to facilitate the identification of small molecules that modulate PRDM proteins. This work will help progress the development of chemical biology tools needed to probe this class of enzyme.

EXPERIMENTAL PROCEDURES

Expression and purification of recombinant PRDM9—Recombinant plasmid of the PR/SET domain of PRDM9 without zinc fingers or knuckle was constructed (Fig. 1). Briefly, the gene encoding residues 192-377 of PRDM9 was cloned from full length mouse PRDM9 (GenBank Accession Number Q96EQ9), fused with a TEV-protease cleavage site preceeded by an N-terminal hexa-histidine tag, and inserted into bacterial expression vector pNIC28-Bsa4 (GenBank Accession Number EF198106). The plasmid was transformed into an *E. coli* BL21-DE3 Rosetta strain (developed by the Protein Production Platform of Nanyang Technological University, Singapore) and expressed using a large-scale expression system (Harbinger Biotech, LEX). Overnight culture was transferred into antibiotic-containing Terrific Broth supplemented with 17 mM KH_2PO_4 and 72 mM K_2HPO_4. Induction of expression was performed at 16°C by adding isopropyl 1-thio-β-D-galactopyranoside to a final concentration of 0.5 mM when Abs_{600} reached 2.0. Expression was allowed to proceed overnight and cells were harvested by centrifugation at 9,000 X *g* for 20 minutes at 4°C, followed by sonication of cell pellets in 20 mM HEPES (pH 7.5), 500 mM NaCl, 0.5 mM TCEP, 1.25 mg/ml lysozyme and protease inhibitors (Roche, cOmplete mini EDTA-free). Cell lysate was clarified by centrifugation at 30,000 X *g* for 30 minutes at 4°C, and the supernatant was loaded onto a 5-ml IMAC column for affinity purification (BioRad, Profinia), followed by size-exclusion chromatography using a HiLoad 16/60 Superdex 200 column (GE Healthcare, AKTA Express). Site-directed mutagenesis of cysteine to proline at residue 321 was performed using a synthetic primer, 5'-GAGGTATGTGAACCCTGCCCGGGATGATG-

3' (GenScript). The bases that were changed to create the desired mutation are underlined. Mutant PRDM9 was recombinantly expressed and purified in similar fashion as the wild type.

Histone substrates—Recombinant *Xenopus laevis* histone octamers (supplemental Fig. S1C and D) were expressed from a single poly-cistronic vector and purified under non-denaturing conditions as previously described (14). Recombinant human full-length histones H2A, H2B, H3 and H4 were purchased from New England Biolabs (M2502S, M2505S, M2503S and M2504S). H3 peptide 1-21 (amino acid sequence ARTKQTARKSTGGKAPRKQLA), H3 peptide 21-44 (amino acid sequence ATKAARKSAPATGGVKKPHRYRPG), and H4 peptide 1-36 (amino acid sequence SGRGKGGKGLGKGGAKRHRKVLRDNIQGIT KPAIRR) were synthesized by GenScript.

Bioluminescent methyltransferase assay—Enzyme activity was measured using a low-volume, bioluminescent assay (Promega CS175601, Methyltransferase-Glo™) in which a light signal is produced from any methyltransferase reaction that uses SAM as cosubstrate. Reaction buffer consisted of 50 mM Tris (pH 8.0) with 20 mM KCl, 5 mM $MgCl_2$, 2 mM DTT and 10% glycerol. For biochemical characterization studies, at least 10 µl of reaction was incubated at 30°C for 60 minutes in PCR tubes, followed by transfer of 4 µl of reaction to duplicate wells in a 384-well plate (Greiner 784075). Low-volume reactions for the high-throughput screen format were incubated at 30°C for 90 minutes directly in the 384-well plate at 4 µl per well. Reaction signals were detected using microplate readers on luminescent mode (Tecan, Safire and M1000). For K_m measurements, reactions were performed at different concentrations of the substrate of interest, and parameters were determined by non-linear regression (GraphPad Prism version 5.03). SAH/SAM conversion curves were created to determine k_{cat} values for each reaction. Enzyme concentrations were set within a range which gave linear product formation. For wild type PRDM9 reactions with histone octamer, H3 protein, H3 peptide 1-21 and H4 peptide 1-36, enzyme concentrations used were 50 nM, 100 nM, 10 nM and 300 nM respectively. 5 µM of mutant PRDM9 was used in reaction with H3 peptide 1-21 to achieve significant background over noise. Drug response studies were performed at 180 nM PRDM9, 2.5 µM H3 peptide 1-21 and 4 µM SAM. All compound stock solutions were prepared in 90% DMSO, of which 5 to 200 nl were transferred to the assay plate using an automated liquid handler (Labcyte, Echo). Enzyme and compounds were pre-incubated in the plate for 30 minutes before addition of substrate. Suramin and sinefungin were purchased from Sigma (S2671 and S8559). Assay robustness was evaluated using a compound library (Microsource, Pharmakon) consisting of five 384-well assay plates, with each plate containing 320 compounds (screened at 12.5 µM), 32 wells of DMSO controls (vehicle controls, up to 5% DMSO) and 32 wells of inhibition controls (1 mM suramin). The intra plate controls were used to measure assay performance and compound biological activity (% inhibition) according to Equations 1 to 3.

$$\text{Signal to noise} = \frac{\text{DMSO control}}{\text{Inhibition control}} \quad (1)$$

$$Z' = 1 - \frac{3 \text{ X } SD_{\text{DMSO control}} + 3 \text{ X } SD_{\text{Inhibition control}}}{\text{Abs}(\text{Mean}_{\text{DMSO control}} - \text{Mean}_{\text{Inhibition control}})} \quad (2)$$

$$\% \text{ inhibition} = 100\left(1 - \frac{\text{Compound RLU} - \text{Mean}_{\text{Inhibition control}}}{\text{Mean}_{\text{DMSO control}} - \text{Mean}_{\text{Inhibition control}}}\right) \quad (3)$$

Molecular modeling—The PRDM9 X-ray structure (PDB # 4C1Q) (6) was downloaded from the RCSB Protein Databank (www.pdb.org). The structure was prepared using the Protein Preparation Wizard of Maestro version 9.4 (www.schrodinger.com). This included adding hydrogen atoms, assigning bond orders, setting protonation states, removing solvent atoms further than 5 Å from SAH, and optimizing the hydrogen bond network. SAH was replaced with a structure of SAM whereby all the atoms shared with SAH retained their coordinates, and it was verified that the extra methyl group of SAM did not clash with the protein. Cysteine at residue 321 was then mutated to a proline. Finally, both the wild type and the Cys321Pro mutant were subjected to 500 steps of constrained minimization with Macromodel version 10.0 using Polak-Ribiere-Conjugate-Gradient (PRCG) (17), the OPLS2005 force field (18) and GB/SA continuum solvation model (19) with water as solvent. All residues further than 7Å from SAH were constrained using flat-bottomed

Cartesian constraints with a force constant of 100 kJ/mol/Å and a half width of 0 Å.

Isothermal titration calorimetry (ITC)—ITC experiments were conducted using a MicroCal Auto-iTC$_{200}$ instrument (GE Healthcare) at 25°C in 20 mM HEPES (pH 7.5) with 50 mM NaCl. Depending on the binding affinities of the ligands, 0.05 mM of enzyme was loaded in the cell with either 1.0 mM or 2.5 mM of ligand in the titrating syringe. In the case of the enzyme-substrate complex, 500 µM of H3 peptide 1-21 was loaded in the cell alongside the enzyme. A total of 20 injections were performed with a spacing of 120 seconds between each injection. To correct for heat of dilution, mixing enthalpies from titrant solution injections into protein-free ITC buffer were subtracted from all data. Data was analyzed using Origin 7.0 software (Origin Lab Corp.), and affinity was calculated using a one-site binding model.

Differential scanning fluorimetry (DSF)—Thermal stability of PRDM9 was measured using assay conditions of 10 µM recombinant protein, 0 mM to 3 mM SAM, SAH or sinefungin (Sigma A7007, A9384 and S8559) and SYPRO Orange (Sigma S5692). Assay buffer consisted of 20 mM HEPES (pH 7.5) and 50 mM NaCl. Samples were subjected to an increase in temperature from 25°C to 95°C over a period of 30 minutes. For thermal stability analysis of enzyme-substrate complex, 150 µM of H3 peptide 1-21 was incubated with enzyme prior to addition of SAM. The experiment was performed on a Roche 480 real-time PCR machine with fluorescence readings taken at each temperature increment. Fluorescence measurements were plotted using GraphPad Prism version 5.03, and melting curves were generated.

Mass spectrometry (MS)—H3 peptides were analyzed by matrix-assisted laser desorption ionization time-of-flight (MALDI TOF) and MALDI TOF/TOF MS on a 4800 MALDI TOF/TOF mass spectrometer (AB Sciex) in positive ion mode. Samples were adjusted to pH 2.0 with 10% trifluoroacetic acid (TFA) and desalted on a Oasis HLB 1cc Extraction Cartridge (Waters) pre-equilibrated with 0.1% TFA. Wash and elution steps were performed with performed 0.1% TFA and 50% acetonitrile (ACN)/ 0.1% TFA respectively. Desalted peptide solution was spotted onto a stainless steel MALDI plate, overlaid with 5 mg/ml α-Cyano-4-hydroxycinnamic acid matrix solution in 50% ACN and 0.1% TFA, and air-dried. MALDI TOF MS data was recorded over a mass range of 800 Da to 3500 Da. Methylated peptide ions, judged by mass increases of multiples of 14 Da (-CH2) over the corresponding substrate peptide ions, were selected for further MALDI TOF/TOF MS analysis. For tandem MS analysis, a 1 kV MS/MS operating mode was used with relative precursor mass window set at +/- 10 Da. MS/MS acquisition of selected precursors was set to 1000 shots per spectrum with 50 shots per sub-spectrum using fixed laser intensity with a uniformly random spot search pattern. Data was analyzed with the 4000 Series Explorer software (AB Sciex, version 3.7). A standard deviation of 3 was used for removal of noise from the spectra, and b and y series ions were annotated according to the peptide sequences. H4 peptide was analyzed using electrospray ionization (ESI) MS on an LTQ Velos Pro Orbitrap machine (Thermo Scientific) by direct infusion ESI at 3 µl/min through a normal API source. Samples were desalted using a C18 cartridge (Sep-Pak Vac 3cc (200mg), Waters).Wash and elution steps were performed with performed 0.1% formic acid (FA), and 50% ACN/ 0.1% FA respectively. The mass spectrometer was operated using electron transfer dissociation (ETD) with the flowing parameter settings: anion target 1E7 with max injection time 200 ms, Velos Pro ion trap MSn AGC target 1E5 with max injection time 300 ms. ETD fragment ions were recorded in Velos Pro ion trap over a mass range of 50 Da to 2000 Da. The spectra were viewed with Xcalibur version 2.2 (Thermo Scientific) and peaks were annotated manually based on their charge states and sequence. Product size determination of all other substrates was performed on an Agilent 6224 LC/MS TOF system.

RESULTS

Biochemical characterization of PRDM9 methyltransferase activity—Enzymatic activity of recombinant mouse PRDM9 (residues E192-F377) was assessed and quantified in a bioluminescent methyltransferase assay which monitored formation of SAH, the reaction by-product of cosubstrate SAM (supplemental Fig. S15A and B). Three representative H3 substrate forms were utilized for characterization: recombinant histone octamer, recombinant full-length H3 protein, and synthetic H3 peptide 1-21. Reaction conditions for each substrate were optimized to achieve high

signal-to-noise readings suitable for determination of enzyme kinetics.

First, a dose-response experiment was performed with increasing concentrations of recombinant histone octamer (Fig. 2A). The K_m value of PRDM9 for histone octamer was determined to be 0.17 μM (Table 1). A similar dose-response experiment using full-length H3 protein (Fig. 2C) revealed that both histone protein and octamer shared highly similar K_m values (Table 1). In contrast, the K_m value for H3 peptide was more than an order of magnitude higher at 3.21 μM. This suggests that PRDM9 binds octamer and H3 protein with higher affinity than the H3 peptide (Table 1 and Fig. 2E). Given that histones H3 and H4 form a tetramer within the octameric complex, we extended our investigation to include a representative H4 substrate – synthetic H4 peptide 1-36 (Fig. 2G). We found the K_m value for H4 peptide (5.47 μM) comparable with that for H3 peptide (Table 1).

A second set of studies was conducted by titrating SAM instead of substrate, to investigate the affinity of PRDM9 for SAM (Fig. 2B, 2D, 2F and 2H). In general, a trend could be observed whereby K_m values with respect to SAM were consistently higher than those with respect to substrate (Table 1). Notably, the K_m for SAM showed a 10-fold increase when the peptide of H4 rather than H3 was used as substrate. An examination of k_{cat} values revealed that of the substrates tested, PRDM9 exhibited highest catalytic activity in reaction with H3 peptide (Table 1). This was consistent with the fact that H3 peptide reactions required the least amount of enzyme (10 nM) to achieve high signal-to-background assay readings. Based on this analysis, the H3 peptide substrate was selected for further development of an assay to screen small molecule inhibitors of PRDM9.

A PR/SET domain mutation significantly diminishes PRDM9 activity—To further our understanding of structural features governing PRDM9 activity, we performed molecular modelling based on an existing X-ray crystal structure of PRDM9 in complex with SAH and a short H3K4me2 peptide (PDB # 4C1Q) (6). SAH was manually replaced by SAM, and the resulting complex was subject to constrained energy minimization (Fig. 3A). Close examination of the PR/SET domain showed that the amino acid backbone of cysteine residue 321 formed two hydrogen bonds with the adenosyl moiety of SAM (Fig. 3A). In certain members of the PRDM family for which intrinsic methyltransferase activity has yet to be demonstrated (e.g. PRDM1 and PRDM10), this position carries a proline residue instead of cysteine (supplemental Fig. S2). We hypothesized that replacing Cys321 with Pro321 in PRDM9 (PRDM9-C321P) would disrupt SAM interactions, since the backbone of proline would not be able to form the hydrogen bonds observed in the wild type X-ray structure. The structure complex of PRDM9-C321P with SAM and H3K4me2 was subject to constrained energy minimization. We observed a rotation of the adenosyl moiety of SAM away from Pro321 due to steric repulsion from the proline ring (Fig. 3B). As a result, no hydrogen bonds between Pro321 and SAM were formed. However, not all SAM interactions were affected by the mutation – the methionine moiety of SAM was still favorably positioned to form hydrogen bonds with Leu258 and Tyr291 (Fig. 3B).

Based on the structural model, we predicted that a single Cys321Pro mutation would weaken PRDM9 catalytic activity through disruption of interactions with SAM. A mutant Cys321Pro construct of PRDM9 was generated through site-directed mutagenesis of the wild type construct, and recombinant PRDM9-C321P enzyme was expressed and purified (supplemental Fig. S1A and B). We assessed PRDM9-C321P methyltransferase activity using the earlier described biochemical assay. Our first attempts to characterize PRDM9-C321P reactions with H3 peptide were conducted using assay conditions similar to those for the wild type. However, these resulted in no detectable activity (data not shown). A direct comparison of the wild type and mutant enzyme dose-response curves revealed that wild type PRDM9 exhibited a linear increase in activity between enzyme concentrations 0 nM to 80 nM, whereas no activity was detected for the mutant enzyme at the corresponding concentration range (supplemental Fig. S3A). Rather, enzyme concentrations over two orders of magnitude higher ($\geq$ 5 μM), were required for significant mutant activity to become apparent (supplemental Fig. S3B). Biochemical characterization of PRDM9-C321P activity was subsequently carried out using 5 μM of enzyme (supplemental Fig. S3C and D). The weakened catalytic activity resulting from the Cys321Pro mutation was further emphasised by the striking

decrease in k_{cat} values of over 500-fold from wild type PRDM9 (Table 1).

Biophysical characterization of PRDM9—Binding properties of wild type and mutant PRDM9 were characterized using ITC. PRDM9 and PRDM9-C321P bound H3 peptide substrate with dissociation constants of 17.6 μM and 31.5 μM respectively, while PRDM9 bound SAM with a dissociation constant of 42.6 μM (Table 2 and Fig. 4A – C). Conversely, no binding between PRDM9-C321P and SAM was detectable. Through DSF analysis, we demonstrated that PRDM9-C321P had a decreased thermal stability of 2°C compared to wild type PRDM9, suggesting an adverse effect on structural integrity caused by the mutation (supplemental Fig. S4). In addition, we observed significantly weaker thermal shifts for PRDM9-C321P (Fig. 5B, black) as compared to the wild type (Fig. 5A, black) in response to SAM. On the other hand, differences between PRDM9 and PRDM9-C321P thermal shifts in response to H3 peptide were comparatively less pronounced (Fig. 5C). The biophysical data described above reiterates the importance of residue Cys321 in facilitating PRDM9 interactions with SAM. Two SAM analogues, SAH and sinefungin (supplemental Fig. S15B and C), were also investigated for binding to PRDM9 and PRDM9-C321P. No significant thermal shift was observed for SAH with both enzymes (Fig. 5A and B, blue). Sinefungin binding resulted in modest thermal shifts for the wildtype, and none for the mutant (Fig. 5A and B, red).

Until recently, all available X-ray crystal structures for PRDM family proteins lacked bound cosubstrate or substrates (e.g. PRDM2 (20), PRDM11 and PRDM12; PDB # 2QPW, 3RAY and 3EP0 respectively). Wu et al. (6) described the first reported PRDM-family ternary structure complex (PDB # 4C1Q) involving PRDM9, SAH and H3 peptide as earlier mentioned. It was further proposed that in the absence of substrate and cosubstrate molecules, PRDM9 would undergo structural rearrangement resulting in an auto-inhibited state (6). Notably, in an earlier unbound crystal of PRDM9 (PDB # 4IJD), the post-set domain structure was incomplete. We hypothesized that events involving PRDM9 substrate and cosubstrate binding were closely related, and that binding at one site of the enzyme would create favorable conditions for binding at the other.

We tested this hypothesis using ITC as a tool to measure thermodynamic Gibbs free energy changes (ΔG) in response to PRDM9 substrate and cosubstrate binding. Data from two experiments were compared: 1) SAH binding with uncomplexed PRDM9, and 2) SAH binding with PRDM9 complexed with H3 peptide 1-21. While no thermodynamic changes were observed for uncomplexed PRDM9 (data not shown), a strong binding curve was generated between SAH and the PRDM9/H3 peptide complex (Fig. 4D). Highly negative ΔG values indicated favorable or spontaneous binding between SAH and PRDM9 when its substrate binding site was occupied (Fig. 4D). This finding was corroborated using DSF as a second biophysical approach, with the actual cosubstrate SAM as a binding partner. Thermal shifts for wild type PRDM9 (Fig. 5A, black) were qualitatively compared with those for the PRDM9/H3 peptide complex in response to SAM (Fig. 5A, green). Complexed PRDM9 showed more significant thermal shifts with increasing concentrations of SAM as compared with PRDM9 alone. Not surprisingly, this trend was not observed in the case of PRDM9-C321P (Fig. 5B, black and green), since the mutation had been specifically designed to interfere with SAM binding. The above results lend biophysical support to the hypothesis that substrate binding to PRDM9 creates favorable conditions for its interaction with SAM.

Molecular characterization of histone substrate modification—Having demonstrated active methylation of histone octamers by PRDM9 in a biochemical assay (Table 1), we proceeded to identify which core histone units of the octamer were modified. Molecular characterization of substrate modification was performed by mass spectrometry analysis to determine the methylation status of each histone protein. Individual histone peaks were clearly identifiable and well-separated in ESI-TOF mass spectra for the unmodified octamer (supplemental Fig. S1D). In our analyses of octamer reaction product formation, we observed a time and enzyme dependent increase in methylation of all four core histone units H2A, H2B, H3 and H4 (supplemental Fig. S5 – 7). Of these, PRDM9 showed the greatest propensity for methylating H3 within the octamer (Table 3).

Similar molecular characterization was performed on the individual histone recombinant proteins H2A, H2B, H3 and H4. Again, we

observed methylation of all core histones by PRDM9 (supplemental Fig. S8), with the H3 substrate being the most highly modified (Table 3). No modification of substrate was detected in any reactions involving PRDM9-C321P (data not shown), leading us to conclude that the Cys321Pro mutation had completely abolished methylation of whole histone proteins. The enzymatic behaviour of PRDM9 appears to be the same whether presented with octamer or individual histone protein as substrate (Fig. 6A).

It is known that methylation of N-terminal histone tails in the nucleosome regulate gene expression. The histone tail length for H3 is 38 residues, and that for H4 is 26 residues (21). With this in mind, we characterized the product formation in PRDM9 reactions with peptides comprising histone tail sequences: H3 peptide 1-21 and H3 peptide 21-44, as well as H4 peptide 1-36. In reactions consisting of excess enzyme and SAM, all histone peptide substrates were modified within the first hour (Fig. 6B – D). Clear conversion of substrate to methylated product could be observed from the mass spectra of each peptide (Fig. 6B – D). Interestingly, the combined maximum methylation observed for both H3 peptides came close to that for whole H3 protein alone (Table 3).

Hayashi et al. previously reported that PRDM9 activity was restricted to H3K4me2, while Wu et al. more recently described mono-, di- and tri-methylation of H3K4, as well as possible methylation of H3K9 (5,6). The number of methylations reported for H3 in Table 3 had been based on saturating reaction conditions, and hence were representative of the highest enzymatic activity *in vitro*. We explored H3 peptide 1-21 substrate modification under controlled conditions that were determined by scaling respective K_m values for substrate and cosubstrate based on the PRDM9 concentration used in the bioluminescent methyltransferase assay. In contrast to the previous saturating reaction (Fig. 6B), not all H3 peptide was fully modified in this case (Fig. 7B). The formation of +1 Me, +2 Me and +3 Me product was observed similar to that previously reported (6). In this study, we have attempted to unequivocally identify this methylation site in H3, using H3 peptide 1-21 containing four lysine residues at K4, K9, K14 and K18. Using MALDI TOF/TOF MS, we demonstrated categorically that H3K4 was mono-, di-, and tri-methylated by PRDM9 (supplemental Fig. S11). Time point analysis showed that this particular methylation pattern was achieved within minutes, and that extending reaction time up to 3 hours did not result in formation of new product (supplemental Fig. S9). With the mutant enzyme PRDM9-C321P, only the mono-methylated H3K4 product was detectable (Fig. 7C and supplemental Fig. S10). MALDI TOF/TOF MS analysis of the earlier described H3 peptide 1-21 reaction under saturating conditions of enzyme and SAM (Fig. 6B) revealed additional methylation sites at K9 and K18 (supplemental Fig. S12).

Having demonstrated the use of MS/MS in the identification of specific histone methylation sites on a H3 peptide, we analysed a peptide representative of the histone tail of H4. The H4 peptide 1-36 had earlier been characterized for substrate modification under saturating PRDM9 reaction conditions (Fig. 7D). As was the case for the H3 peptide, scaling down the H4 peptide reaction to more controlled conditions resulted in less product formation. At low levels of SAM, only the mono-methylated product of H4 peptide was apparent (supplemental Fig. S13). Using ESI ETD MS/MS analysis, we identified the methylation site to be H4K20me (supplemental Fig. S14), a mark often linked to transcriptional repression (15). The di-methylated product was detectable at higher levels of SAM (supplemental Fig. S13).

Inhibition assay and compound library screen—A low-volume inhibition assay for PRDM9 was optimized based on the earlier described biochemical assay and dose-response studies were performed. We found that suramin (supplemental Fig. S15D), a known histone methyltransferase inhibitor (22), inhibited PRDM9 with a reproducible IC_{50} of 50.5 ± 26.5 μM (Fig. 8A). Sinefungin, a fungal compound and analog of SAM, gave a less potent IC_{50} of 357.3 ± 61.9 μM (Fig. 8B). In order to evaluate assay performance and robustness, we applied a high-throughput screen format to the assay using a small library of 1,600 bioactive compounds. Several hits were observed whereby 12.5 μM of compound gave rise to more than 40% inhibition (Fig. 8C). Assay signal-to-noise was consistently above 9.5 (supplemental Table S1), a satisfactory window for distinguishing between active and inactive compounds. Another measure of assay robustness, the *Z'* factor, was determined to account for variability in the maximum and baseline signals.

The average *Z'* factor (> 0.72) among all the plates screened met the acceptance criteria for assay validation (23). The indicators described demonstrate the robustness and reproducibility of this assay for evaluating PRDM9-modulating compounds. Significantly, we have taken the first step towards screening a larger chemical space to find a pharmacologically viable probe for PRDM proteins.

DISCUSSION

Several recent studies have highlighted the role of PRDM9 in meiotic progression, providing important insight into molecular mechanisms underlying recombination initiation (11,24-26). In *PRDM9*-deficient mouse testis, impaired meiotic gene transcription was observed with a concurrent decrease in H3K4 trimethylation (5). The enrichment of H3K4me3 at yeast and mouse initation sites provided further evidence for epigenetic control of recombination hotspot specification (27-29). Consequently, the H3K4 methyltransferase activity of PRDM9 has been an area of significant interest (6,30,31).

Our findings show that the propensity of PRDM9 to catalyze histone lysine methylation is far more extensive than previously recognized. We have characterized the activity of recombinantly expressed PRDM9 using a broad range of histone substrates – including histone octamers, whole histones and histone peptides – and demonstrated, for the first time, that PRDM9 methylates all four core histone units H2A, H2B, H3 and H4. A comparison of substrate modification under standardized reaction conditions revealed that methylation of H3 was most prevalent among the four core histones. We performed further molecular characterization of H3 and H4 peptides which were representative of amino-terminal histone tails commonly subject to post-translational modifications. MS/MS analysis of site-specific histone modification presented indisputable evidence that H3K4 was mono-, di- and tri-methylated by PRDM9. Interestingly, two additional lysines on the H3 peptide, H3K9 and H3K18, were observed to have undergone di- and mono-methylation respectively in the same enzymatic reaction. In the case of the H4 peptide, another novel methylation site was detected at H4K20, which had undergone mono- and di-methylation.

The identification of novel histone substrates of PRDM9 opens up new possibilities for its involvement in additional epigenetic processes. While not much is known about the role of H3K18 methylation, di-methylated H3K9 and H4K20 are well-characterized histone marks associated with transcriptionally silent or repressed genes, while H3K4me3 is a hallmark of transcriptionally active genes (15). Some members of the PRDM family show strong context dependency and bidirectional transcriptional activity, e.g. PRDM2 action in response to oestrogen levels, and PRDM16 function during brown fat specification (7,32,33). The concomitant occurrence of activating and repressive marks mediated by PRDM9 raises the question of whether it can exhibit diverse functions under different cellular conditions. Another point to consider is the physiological relevance of these novel methylation sites. While PRDM9-mediated H3 methylation is reasonably well-understood in the context of meiotic hotspot localization, the biological functions of H2A, H2B and H4 methylation by PRDM9 are unknown. It would be premature to conclude if novel histone substrates methylated by PRDM9 under *in vitro* conditions would display the same modifications under physiological or pathological settings. Until further investigation is performed, there also remains the possibility that substrate recognition of PRDM9 could extend to non-histone proteins, as has been demonstrated for other histone lysine methyltransferases such as SMYD2 (non-histone substrate p53) and NSD1 (non-histone substrate NFκb) (34).

Although the PRDM family members have been implicated in multiple disease and developmental processes, relatively little is known about their mechanisms of action. To date, intrinsic methyltransferase activity has been demonstrated only for a few members of the family (e.g. PRDM2, -8 and -9) (7,8). To better understand structural features governing PRDM9 methyltransferase activity, we designed and engineered a PR/SET domain mutant of PRDM9, utilizing a systematic approach comprising sequence alignment, molecular modelling and rational site-directed mutagenesis. Our biochemical data revealed that the introduced mutation, Cys321Pro, was able to cause significant reduction in PRDM9 catalytic activity; this was predicted to be a result of disrupted SAM binding. Using biophysical

methods, we have demonstrated that the ability of mutant PRDM9 to bind SAM was indeed compromised to a significant degree as compared to the wild type.

PRDM proteins differ from other histone lysine methyltransferases in their PR/SET domains, which share only 20–30% sequence identity with classical SET domains (8,35). While SET domain methyltransferases have frequently been co-crystallized with SAM, no similar co-crystal structures have been reported for the PRDM family. Remarkably, all available PRDM family structures are in the unbound form, with the exception of a PRDM9/H3 peptide/SAH co-crystal structure (6). Interestingly, the unbound structure of PRDM9 displayed a conformational change in the post-set domain which resulted in a possible autoinhibited state (6). Based on the above observations, we speculated that histone substrate binding of PRDM9 selected for a conformation favorable for SAM binding. We utilized the loss-of-binding PR/SET domain mutant of PRDM9 as a tool for further investigation. Clear increases in SAM and SAH binding were observed when wild type PRDM9 was pre-complexed with a H3 peptide substrate in ITC and DSF experiments, compared with binding to the enzyme alone. No increase in binding was observed when the PRDM9 mutant was pre-complexed with the substrate. Our data provides biophysical evidence that PRDM9 shows greater propensity for SAM binding when its histone substrate binding site is occupied, and corroborates the structural observations of Wu et al. (6). Further investigation of this structural phenomenon in other members of the PRDM family could steer new approaches for the formation of high resolution co-crystal structures.

The close relationship between SAM and histone substrate binding is further reflected in our enzyme kinetics characterization, whereby a range of SAM affinities were observed for different histone substrate reactions with PRDM9. For example, while both H3 and H4 peptides displayed similar substrate-binding affinities for PRDM9, the K_m value for SAM was ten-fold higher for the H4 peptide. An earlier report showed efficient PRDM9 methylation of H3 peptides in a coupled fluorescent assay, but no methylation of H4K20 peptide (6). This can be explained by the higher K_m value for SAM in the H4 reaction, which suggests that higher SAM concentrations would be needed for detectable activity.

Epigenetic drug development has gained considerable interest in light of recent progress in small-molecule modulation of methylation-dependent pathways. Selective inhibitors of two histone lysine methyltransferases, EZH2 and DOT1L, have shown efficacy in preclinical proof-of-concept studies and entered Phase I clinical trials for diffuse large B-cell and follicular lymphoma, and MLL-rearranged leukemia, respectively (36,37). These successes bring to the fore the potential of other histone lysine methyltransferases, including the PRDM family, as novel epigenetic drug targets. A body of work has described the emerging roles of PRDM proteins in diverse cancer types, including leukemia, breast cancer and stomach cancer. Currently, the disease biology and mechanisms of action for the PRDM family are not well-understood (7,8). In order to ascertain their therapeutic relevance and identify opportunities for pharmacological modulation, further characterization of PRDM proteins would be needed.

Through a combination of biochemical, biophysical and chemical biology techniques, we have characterized a prototype member of the PRDM family, PRDM9, and acquired fresh perspective about its enzymatic action. In addition, we have optimized a robust biochemical assay for PRDM9 and demonstrated its chemical tractability through a small library screen of bioactive compounds. The application of this assay to a high throughput screen format can facilitate the generation of small molecule chemical probes for this protein family. It is our hope that this work will pave the way to the discovery of small drug-like molecules/chemical biology probes which the community can use to explore new therapeutic opportunities for the PRDM family.

REFERENCES

1. Ancelin, K., Lange, U. C., Hajkova, P., Schneider, R., Bannister, A. J., Kouzarides, T., and Surani, M. A. (2006) Blimp1 associates with Prmt5 and directs histone arginine methylation in mouse germ cells. *Nature cell biology* **8**, 623-630
2. Davis, C. A., Haberland, M., Arnold, M. A., Sutherland, L. B., McDonald, O. G., Richardson, J. A., Childs, G., Harris, S., Owens, G. K., and Olson, E. N. (2006) PRISM/PRDM6, a transcriptional

repressor that promotes the proliferative gene program in smooth muscle cells. *Molecular and cellular biology* **26**, 2626-2636
3. Kim, K. C., Geng, L., and Huang, S. (2003) Inactivation of a histone methyltransferase by mutations in human cancers. *Cancer research* **63**, 7619-7623
4. Eom, G. H., Kim, K., Kim, S. M., Kee, H. J., Kim, J. Y., Jin, H. M., Kim, J. R., Kim, J. H., Choe, N., Kim, K. B., Lee, J., Kook, H., Kim, N., and Seo, S. B. (2009) Histone methyltransferase PRDM8 regulates mouse testis steroidogenesis. *Biochemical and biophysical research communications* **388**, 131-136
5. Hayashi, K., Yoshida, K., and Matsui, Y. (2005) A histone H3 methyltransferase controls epigenetic events required for meiotic prophase. *Nature* **438**, 374-378
6. Wu, H., Mathioudakis, N., Diagouraga, B., Dong, A., Dombrovski, L., Baudat, F., Cusack, S., de Massy, B., and Kadlec, J. (2013) Molecular basis for the regulation of the H3K4 methyltransferase activity of PRDM9. *Cell reports* **5**, 13-20
7. Hohenauer, T., and Moore, A. W. (2012) The Prdm family: expanding roles in stem cells and development. *Development* **139**, 2267-2282
8. Fog, C. K., Galli, G. G., and Lund, A. H. (2012) PRDM proteins: important players in differentiation and disease. *BioEssays : news and reviews in molecular, cellular and developmental biology* **34**, 50-60
9. Morishita, K. (2007) Leukemogenesis of the EVI1/MEL1 gene family. *International journal of hematology* **85**, 279-286
10. Schneider, R., Bannister, A. J., and Kouzarides, T. (2002) Unsafe SETs: histone lysine methyltransferases and cancer. *Trends in biochemical sciences* **27**, 396-402
11. Baudat, F., Buard, J., Grey, C., Fledel-Alon, A., Ober, C., Przeworski, M., Coop, G., and de Massy, B. (2010) PRDM9 is a major determinant of meiotic recombination hotspots in humans and mice. *Science* **327**, 836-840
12. Hochwagen, A., and Marais, G. A. (2010) Meiosis: a PRDM9 guide to the hotspots of recombination. *Current biology : CB* **20**, R271-274
13. Feichtinger, J., Aldeailej, I., Anderson, R., Almutairi, M., Almatrafi, A., Alsiwiehri, N., Griffiths, K., Stuart, N., Wakeman, J. A., Larcombe, L., and McFarlane, R. J. (2012) Meta-analysis of clinical data using human meiotic genes identifies a novel cohort of highly restricted cancer-specific marker genes. *Oncotarget* **3**, 843-853
14. Shim, Y., Duan, M. R., Chen, X., Smerdon, M. J., and Min, J. H. (2012) Polycistronic coexpression and nondenaturing purification of histone octamers. *Analytical biochemistry* **427**, 190-192
15. Arrowsmith, C. H., Bountra, C., Fish, P. V., Lee, K., and Schapira, M. (2012) Epigenetic protein families: a new frontier for drug discovery. *Nature reviews. Drug discovery* **11**, 384-400
16. Copeland, R. A., Solomon, M. E., and Richon, V. M. (2009) Protein methyltransferases as a target class for drug discovery. *Nature reviews. Drug discovery* **8**, 724-732
17. Polak, E., and Ribiere, G. (1969) Note sur la Convergence de Méthodes de Directions Conjuguées. *Revenue Francaise informat. Recherche opérationelle, Série Rouge* **16**, 35-43
18. Kaminski, G. A., Friesner, R. A., Tirado-Rives, J., and Jorgensen, W. L. (2001) Evaluation and reparametrization of the OPLS-AA force field for protein via comparison with accurate quantum chemical calculations on peptides. *J. Phys. Chem. B* **105**, 6474–6487
19. Hasel, W., Hendrickson, T. F., and Still, W. C. (1988) A rapid approximation to the solvent accessible surface areas of atoms. *Tetrahedron Comput. Method.* **1**, 103-116
20. Wu, H., Min, J., Lunin, V. V., Antoshenko, T., Dombrovski, L., Zeng, H., Allali-Hassani, A., Campagna-Slater, V., Vedadi, M., Arrowsmith, C. H., Plotnikov, A. N., and Schapira, M. (2010) Structural biology of human H3K9 methyltransferases. *PloS one* **5**, e8570
21. Potoyan, D. A., and Papoian, G. A. (2011) Energy landscape analyses of disordered histone tails reveal special organization of their conformational dynamics. *Journal of the American Chemical Society* **133**, 7405-7415

22. Horiuchi, K. Y., Eason, M. M., Ferry, J. J., Planck, J. L., Walsh, C. P., Smith, R. F., Howitz, K. T., and Ma, H. (2013) Assay development for histone methyltransferases. *Assay and drug development technologies* **11**, 227-236
23. Entzeroth, M., Flotow, H., and Condron, P. (2009) Overview of high-throughput screening. *Current protocols in pharmacology / editorial board, S.J. Enna* **Chapter 9**, Unit 9 4
24. Parvanov, E. D., Petkov, P. M., and Paigen, K. (2010) Prdm9 controls activation of mammalian recombination hotspots. *Science* **327**, 835
25. Myers, S., Bowden, R., Tumian, A., Bontrop, R. E., Freeman, C., MacFie, T. S., McVean, G., and Donnelly, P. (2010) Drive against hotspot motifs in primates implicates the PRDM9 gene in meiotic recombination. *Science* **327**, 876-879
26. Grey, C., Barthes, P., Chauveau-Le Friec, G., Langa, F., Baudat, F., and de Massy, B. (2011) Mouse PRDM9 DNA-binding specificity determines sites of histone H3 lysine 4 trimethylation for initiation of meiotic recombination. *PLoS biology* **9**, e1001176
27. Borde, V., Robine, N., Lin, W., Bonfils, S., Geli, V., and Nicolas, A. (2009) Histone H3 lysine 4 trimethylation marks meiotic recombination initiation sites. *The EMBO journal* **28**, 99-111
28. Buard, J., Barthes, P., Grey, C., and de Massy, B. (2009) Distinct histone modifications define initiation and repair of meiotic recombination in the mouse. *The EMBO journal* **28**, 2616-2624
29. Hayashi, K., and Matsui, Y. (2006) [Meiosis-specific histone methylation is essential for meiotic progression]. *Tanpakushitsu kakusan koso. Protein, nucleic acid, enzyme* **51**, 441-445
30. Brick, K., Smagulova, F., Khil, P., Camerini-Otero, R. D., and Petukhova, G. V. (2012) Genetic recombination is directed away from functional genomic elements in mice. *Nature* **485**, 642-645
31. Baudat, F., Imai, Y., and de Massy, B. (2013) Meiotic recombination in mammals: localization and regulation. *Nature reviews. Genetics* **14**, 794-806
32. Carling, T., Kim, K. C., Yang, X. H., Gu, J., Zhang, X. K., and Huang, S. (2004) A histone methyltransferase is required for maximal response to female sex hormones. *Molecular and cellular biology* **24**, 7032-7042
33. Kajimura, S., Seale, P., Tomaru, T., Erdjument-Bromage, H., Cooper, M. P., Ruas, J. L., Chin, S., Tempst, P., Lazar, M. A., and Spiegelman, B. M. (2008) Regulation of the brown and white fat gene programs through a PRDM16/CtBP transcriptional complex. *Genes & development* **22**, 1397-1409
34. Zhang, X., Wen, H., and Shi, X. (2012) Lysine methylation: beyond histones. *Acta biochimica et biophysica Sinica* **44**, 14-27
35. Huang, S. (2002) Histone methyltransferases, diet nutrients and tumour suppressors. *Nature reviews. Cancer* **2**, 469-476
36. Wigle, T. J., and Copeland, R. A. (2013) Drugging the human methylome: an emerging modality for reversible control of aberrant gene transcription. *Current opinion in chemical biology* **17**, 369-378
37. Copeland, R. A. (2013) Molecular pathways: protein methyltransferases in cancer. *Clinical cancer research : an official journal of the American Association for Cancer Research* **19**, 6344-6350

Acknowledgments—We would like to thank the Protein Production Platform (Nanyang Technology University, Singapore) for providing the PRDM9 construct, and Dr Xuezhi Bi (Bioprocessing Technology Institute, A*STAR, Singapore) for his help in the ETD experiment.

FOOTNOTES

*This work was supported by a Joint-Council Office Development Programme grant from A*STAR, Singapore.

FIGURE LEGENDS

FIGURE 1. A. Schematic depiction of the PR/SET domain (yellow), zinc knuckle (green), and zinc fingers (blue) of full-length mouse PRDM9. B. Recombinant mouse PRDM9 construct consisting of the PR/SET domain (yellow) and a hexahistidine tag/TEV protease recognition site (red).

FIGURE 2. PRDM9 enzymatic activities were characterized for a series of histone substrates using an i*n vitro* bioluminescent methyltransferase assay. Substrate and SAM titration curves are shown for wild type PRDM9 reactions using (A-B) histone octamer, (C-D) full- length H3 protein, (E-F) H3 peptide 1-21, and (G-H) H4 peptide 1-36 as substrates. The concentrations of PRDM9 in the reactions were 50 nM, 100 nM, 10 nM and 300 nM respectively.

FIGURE 3. Molecular models showing PR/SET domain interactions. A. PRDM9 wildtype. B. PRDM9-C321P mutant. The PRDM9 X-ray structure (PDB # 4C1Q) was used as a template for SAM docking, which was followed by energy minimization.

FIGURE 4. Biophysical characterization of binding using isothermal calorimetry. A. PRDM9 and H3 peptide 1-21. B. PRDM9 and SAM. C. PRDM9-C321P and H3 peptide 1-21. D. PRDM9/H3 peptide 1-21 and SAH.

FIGURE 5. Differential scanning fluorimetry was performed to measure protein thermal shifts in response to binding. A. Dose response thermal shifts of PRDM with respect to SAM and SAM analogues. B. Dose response thermal shifts of PRDM9-C321P with respect to SAM and SAM analogues. C. Dose response thermal shifts of PRDM9 and PRDM9-C321P with respect to H3 peptide 1-21.

FIGURE 6. A. Bar graph comparison of the maximum methylation numbers observed in H2A, H2B, H3 and H4 derived from histone octamer and histone protein. B-D. Mass spectra of negative controls and PRDM9 reactions for the substrates H3 peptide 1-21, H3 peptide 21-44 and H4 peptide 1-36 respectively. 15 μM peptide, 10 μM of PRDM9 and 1 mM SAM were used in all reactions.

FIGURE 7. Mass spectra show substrate peaks representing (A) H3 peptide 1-21 control, (B) H3 peptide 1-21 methylation by 100 nM PRDM9, and (C) H3 peptide 1-21 methylation by 5μM PRDM9-C31P. 40 μM SAM was used in both reactions.

FIGURE 8. Low-volume inhibition assay for PRDM9. A. Dose-response inhibition by suramin. B. Dose-response inhibition by sinefungin. C. Scatter plot depicting percent inhibition values from a small library screen.

TABLE 1

Kinetic parameters of wild type and mutant PRDM9 activity

Enzymatic activities of wild type and mutant PRDM9 were characterized for a series of histone substrates.

Enzyme	Substrate or Co-substrate	K_m	k_{cat}	k_{cat}/K_m
		μM	s^{-1}	$M^{-1}s^{-1}$
PRDM9	Histone octamer	0.17 ± 0.02	$1.4 \times 10^{-2} \pm 9.6 \times 10^{-5}$	8.6×10^{4}
	SAM*	22.29 ± 1.70	$2.6 \times 10^{-2} \pm 6.7 \times 10^{-4}$	1.2×10^{3}
	H3 protein	0.19 ± 0.02	$3.5 \times 10^{-3} \pm 1.8 \times 10^{-4}$	1.8×10^{4}
	SAM‡	19.01 ± 1.10	$3.9 \times 10^{-3} \pm 7.4 \times 10^{-5}$	2.0×10^{2}
	H3 peptide 1-21	3.21 ± 0.59	$7.1 \times 10^{-2} \pm 3.4 \times 10^{-3}$	2.2×10^{4}
	SAM#	8.23 ± 0.63	$10.7 \times 10^{-2} \pm 1.9 \times 10^{-3}$	1.3×10^{4}
	H4 peptide 1-36	5.47 ± 1.00	$3.0 \times 10^{-3} \pm 9.2 \times 10^{-5}$	5.5×10^{2}
	SAM^	81.66 ± 9.45	$1.9 \times 10^{-3} \pm 8.1 \times 10^{-5}$	22.9
PRDM9-C321P	H3 peptide 1-21	3.49 ± 0.36	$1.4 \times 10^{-4} \pm 2.6 \times 10^{-6}$	39.4
	SAM#	19.19 ± 1.85	$1.4 \times 10^{-4} \pm 4.1 \times 10^{-6}$	7.1

* reaction with histone octamer
‡ reaction with H3 protein
# reaction with H3 peptide 1-21
^ reaction with H4 peptide 1-36

TABLE 2

Measurement of dissociation constants for wild type and mutant PRDM9

Binding of H3 peptide, SAM and SAH to wild type and mutant PRDM9 was investigated using isothermal titration calorimetry.

Enzyme	**Binding Partner**	K_D	**ΔH**	**ΔS**
		μM	*kcal/mol*	*cal/mol/deg*
PRDM9	H3 peptide 1-21	17.6 ± 8.3	-4.3 ± 1.0	7.6 ± 2.3
	SAM	42.6 ± 3.5	-5.6 ± 1.3	1.4 ± 4.3
	SAH	n.d.	n.d.	n.d.
PRDM9-C321P	H3 peptide 1-21	31.5 ± 0.1	-2.0 ± 0.2	13.9 ± 0.7
	SAM	n.d.	n.d.	n.d.
	SAH	n.d.	n.d.	n.d.

n.d.: not detected

TABLE 3

Molecular characterization of PRDM9 substrate modification

PRDM9 substrate modification of histone octamer, histone protein and histone peptide was characterized by ESI-TOF mass spectrometry analysis.

	Substrate	Max. Observed Methylation
Histone octamer*	H2A	1
	H2B	2
	H3	10
	H4	5
Histone protein‡	H2A	6
	H2B	11
	H3	17
	H4	10
Histone peptide#	H3 (1-21)	7
	H3 (21-44)	9
	H4 (1-36)	6

*Reaction consisted of 10 μM PRDM9, 8 μM histone octamer, and 1 mM SAM.
‡ Reaction consisted of 10 μM PRDM9, 15 μM histone protein, and 1 mM SAM.
‡ Reaction consisted of 10 μM PRDM9, 50 μM histone peptide, and 1 mM SAM.

Figure 1

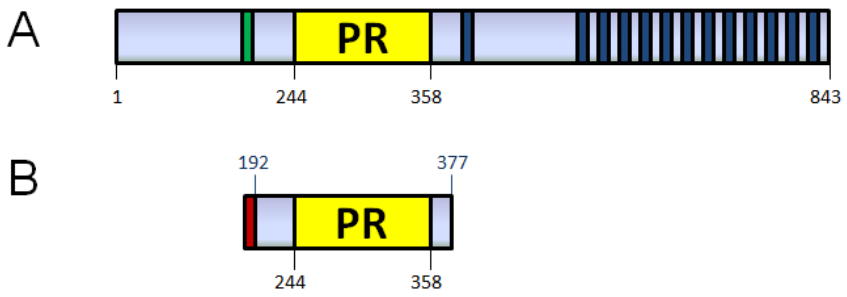

Figure 2

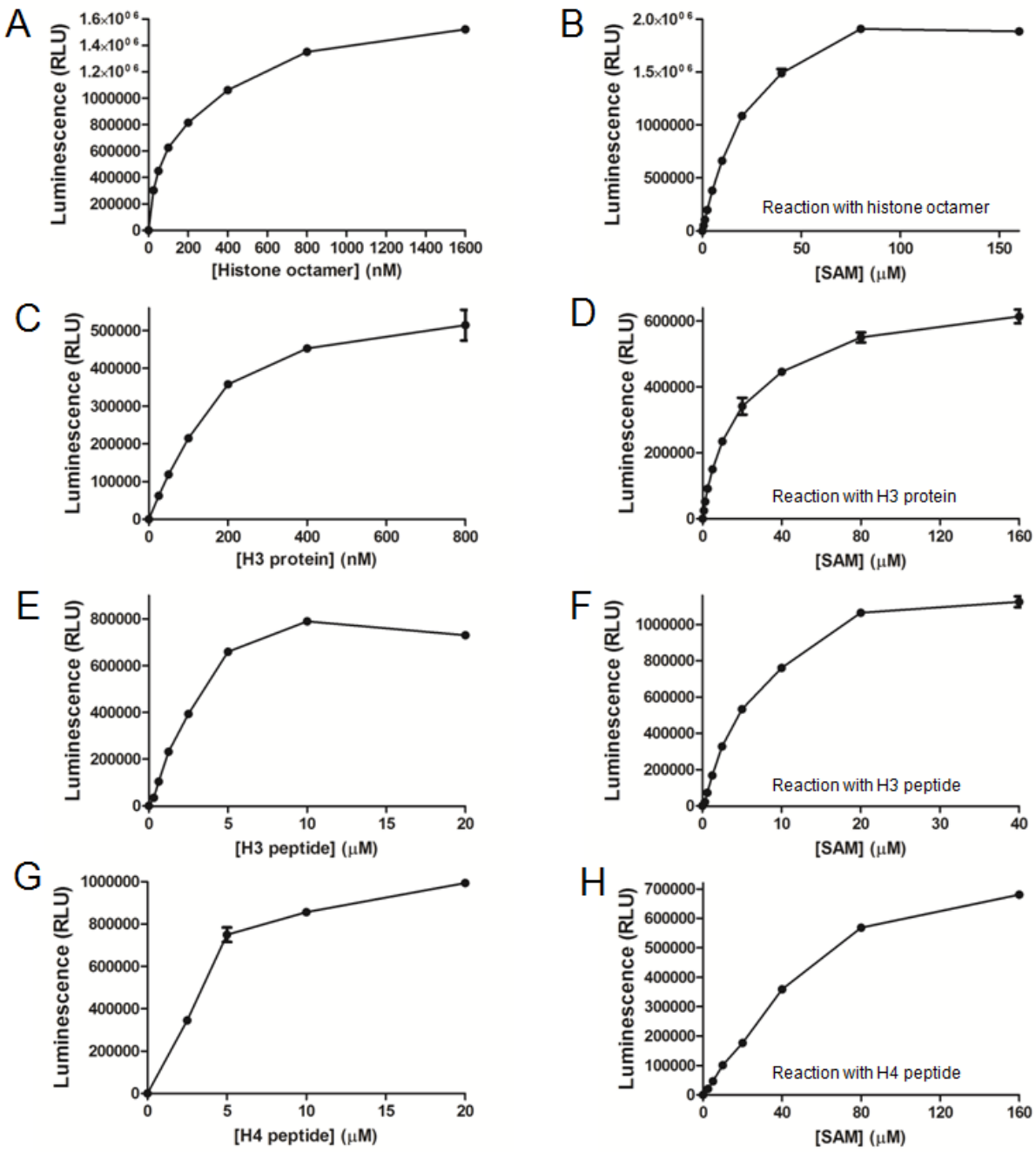
A
Luminescence (RLU)
[Histone octamer] (nM)
B
Luminescence (RLU)
Reaction with histone octamer
[SAM] (μM)
C
Luminescence (RLU)
[H3 protein] (nM)
D
Luminescence (RLU)
Reaction with H3 protein
[SAM] (μM)
E
Luminescence (RLU)
[H3 peptide] (μM)
F
Luminescence (RLU)
Reaction with H3 peptide
[SAM] (μM)
G
Luminescence (RLU)
[H4 peptide] (μM)
H
Luminescence (RLU)
Reaction with H4 peptide
[SAM] (μM)

Figure 3

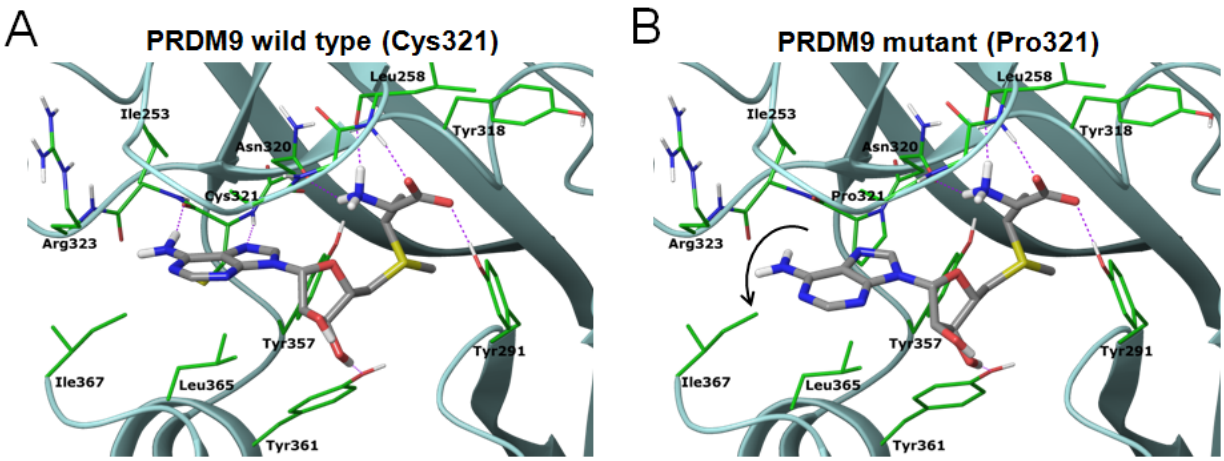
A
PRDM9 wild type (Cys321)
Leu258
Ile253
Tyr318
Asn320
Cys321
Arg323
Tyr357
Tyr291
Ile367
Leu365
Tyr361
B
PRDM9 mutant (Pro321)
Leu258
Ile253
Tyr318
Asn320
Pro321
Arg323
Tyr357
Tyr291
Ile367
Leu365
Tyr361

Figure 4

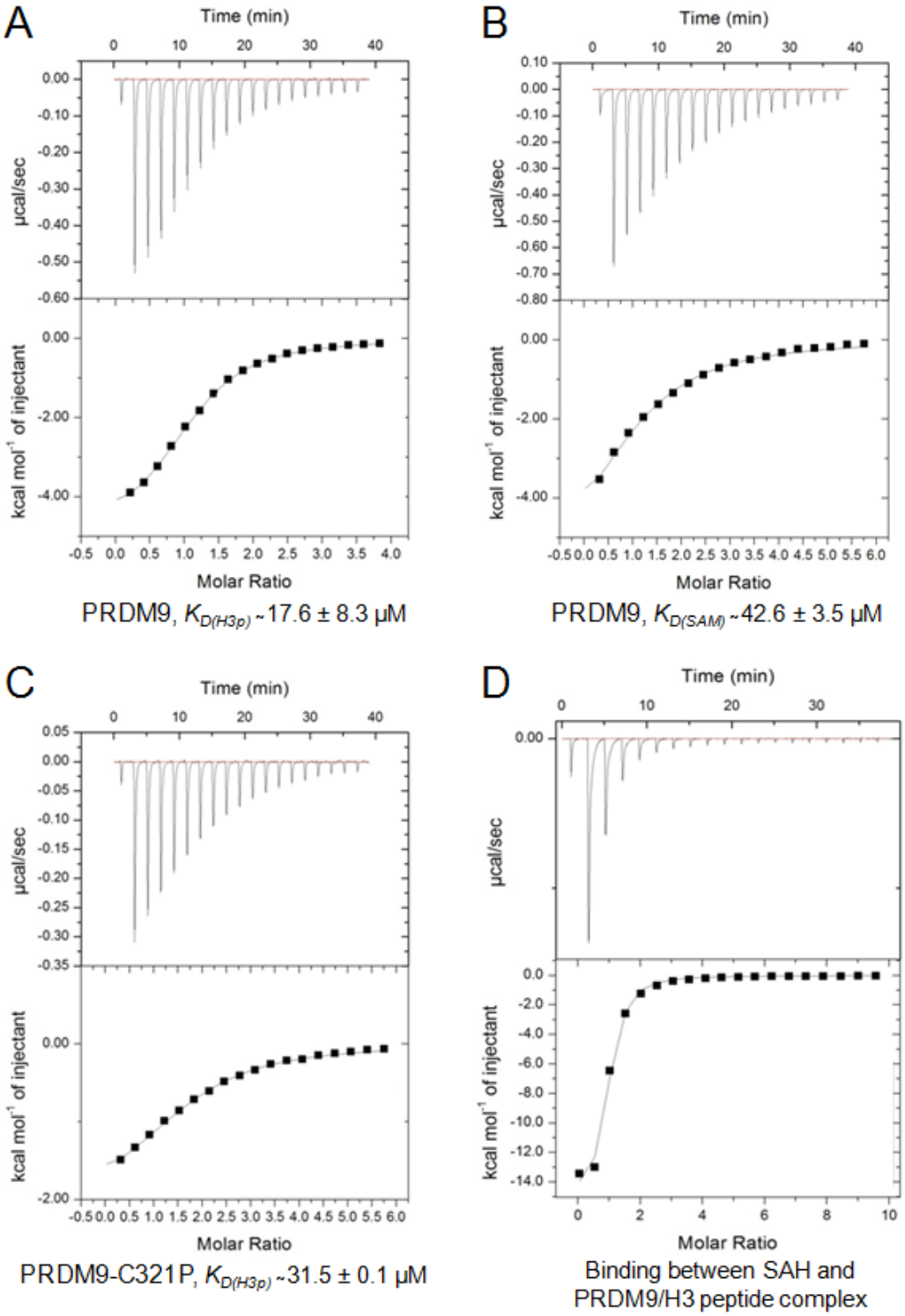
A
Time (min)
µcal/sec
kcal mol⁻¹ of injectant
Molar Ratio
PRDM9, $K_{D(H3p)}$ ~17.6 ± 8.3 µM
B
Time (min)
µcal/sec
kcal mol⁻¹ of injectant
Molar Ratio
PRDM9, $K_{D(SAM)}$ ~42.6 ± 3.5 µM
C
Time (min)
µcal/sec
kcal mol⁻¹ of injectant
Molar Ratio
PRDM9-C321P, $K_{D(H3p)}$ ~31.5 ± 0.1 µM
D
Time (min)
µcal/sec
kcal mol⁻¹ of injectant
Molar Ratio
Binding between SAH and
PRDM9/H3 peptide complex

Figure 5

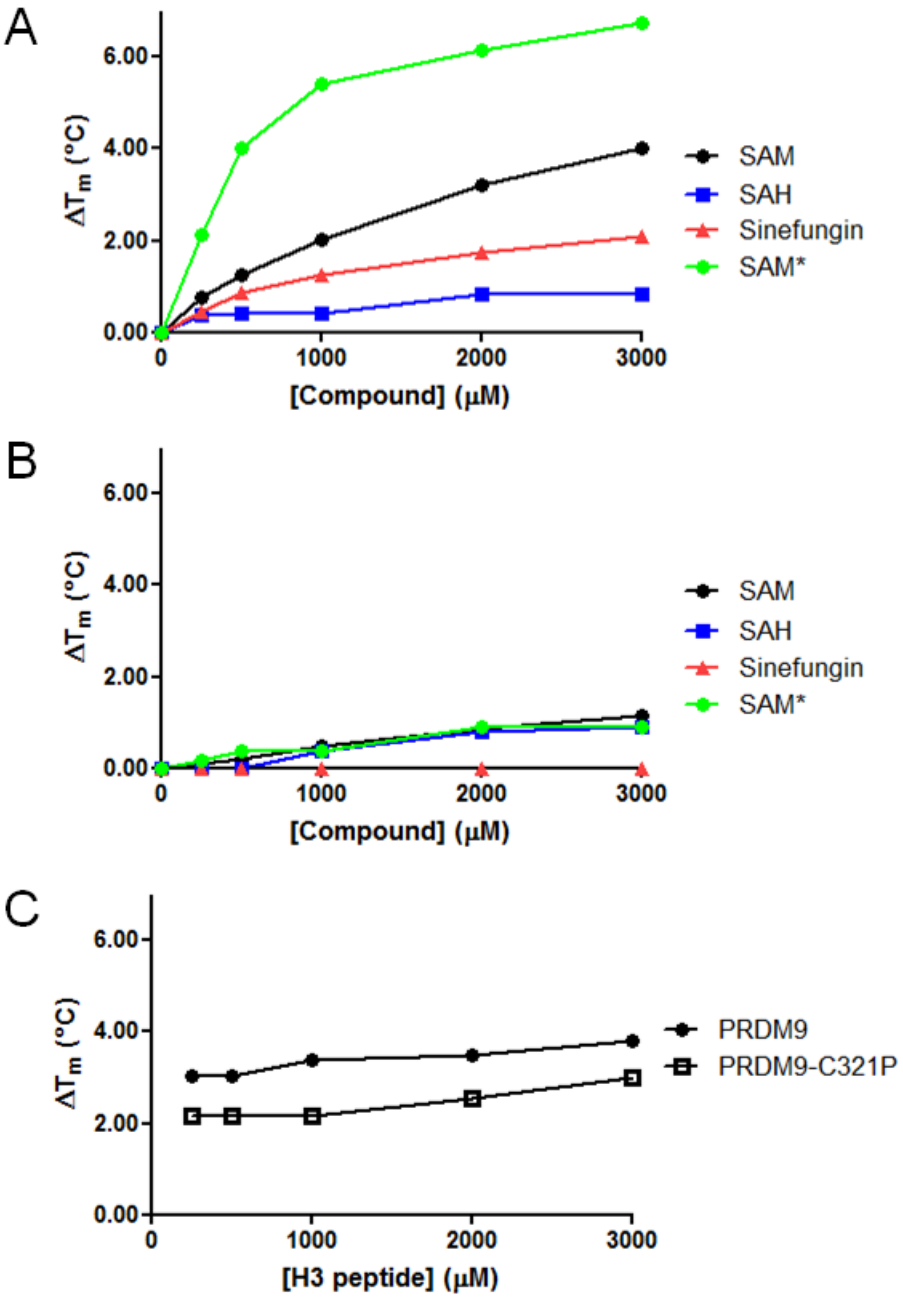
A
6.00
4.00
2.00
0.00
ΔTm (°C)
0
1000
2000
3000
[Compound] (µM)
SAM
SAH
Sinefungin
SAM*
B
6.00
4.00
2.00
0.00
ΔTm (°C)
0
1000
2000
3000
[Compound] (µM)
SAM
SAH
Sinefungin
SAM*
C
6.00
4.00
2.00
0.00
ΔTm (°C)
0
1000
2000
3000
[H3 peptide] (µM)
PRDM9
PRDM9-C321P

Figure 6

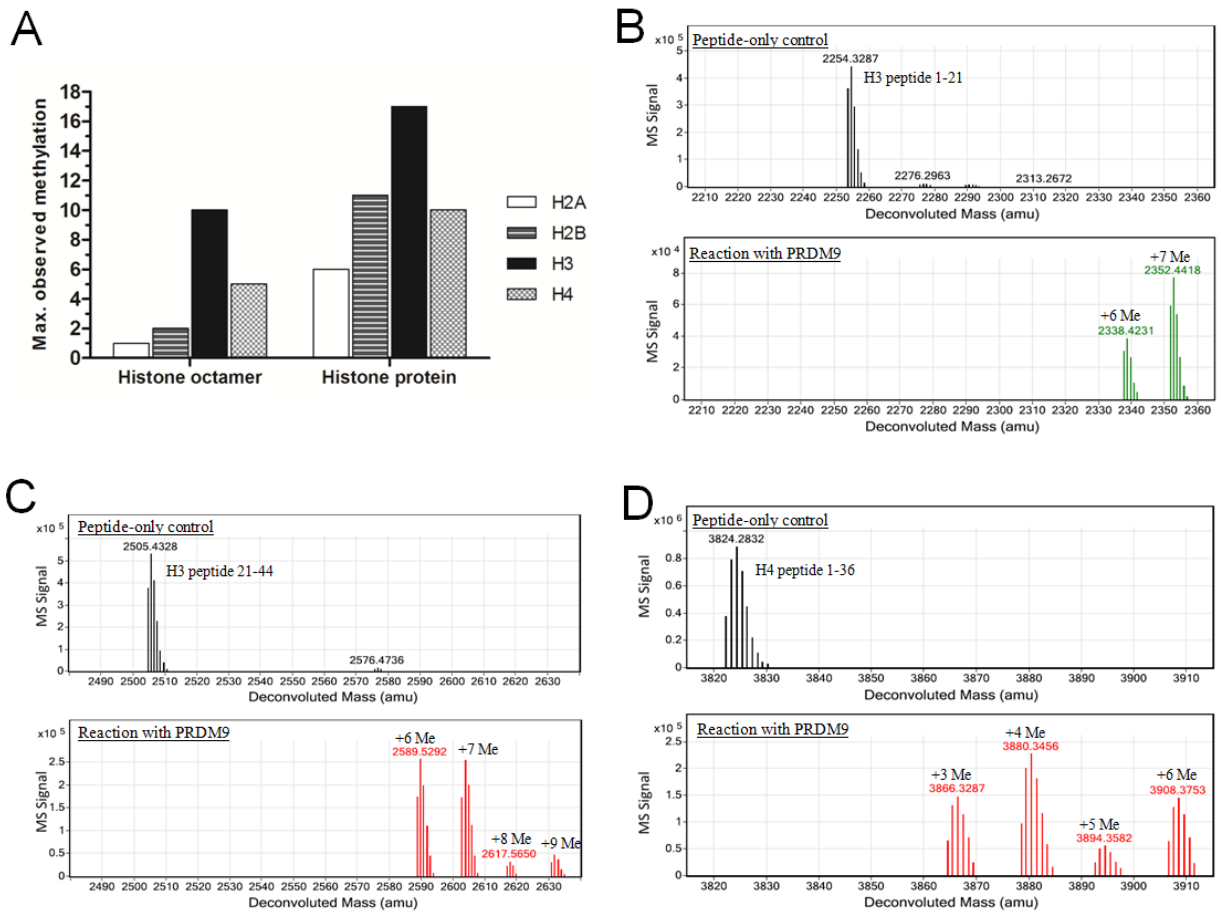
A
Max. observed methylation
Histone octamer
Histone protein
H2A
H2B
H3
H4
B
Peptide-only control
2254.3287
H3 peptide 1-21
2276.2963
2313.2672
MS Signal
Deconvoluted Mass (amu)
Reaction with PRDM9
+6 Me
2338.4231
+7 Me
2352.4418
C
Peptide-only control
2505.4328
H3 peptide 21-44
2576.4736
Reaction with PRDM9
+6 Me
2589.5292
+7 Me
+8 Me
2617.5650
+9 Me
D
Peptide-only control
3824.2832
H4 peptide 1-36
Reaction with PRDM9
+3 Me
3866.3287
+4 Me
3880.3456
+5 Me
3894.3582
+6 Me
3908.3753

Figure 7

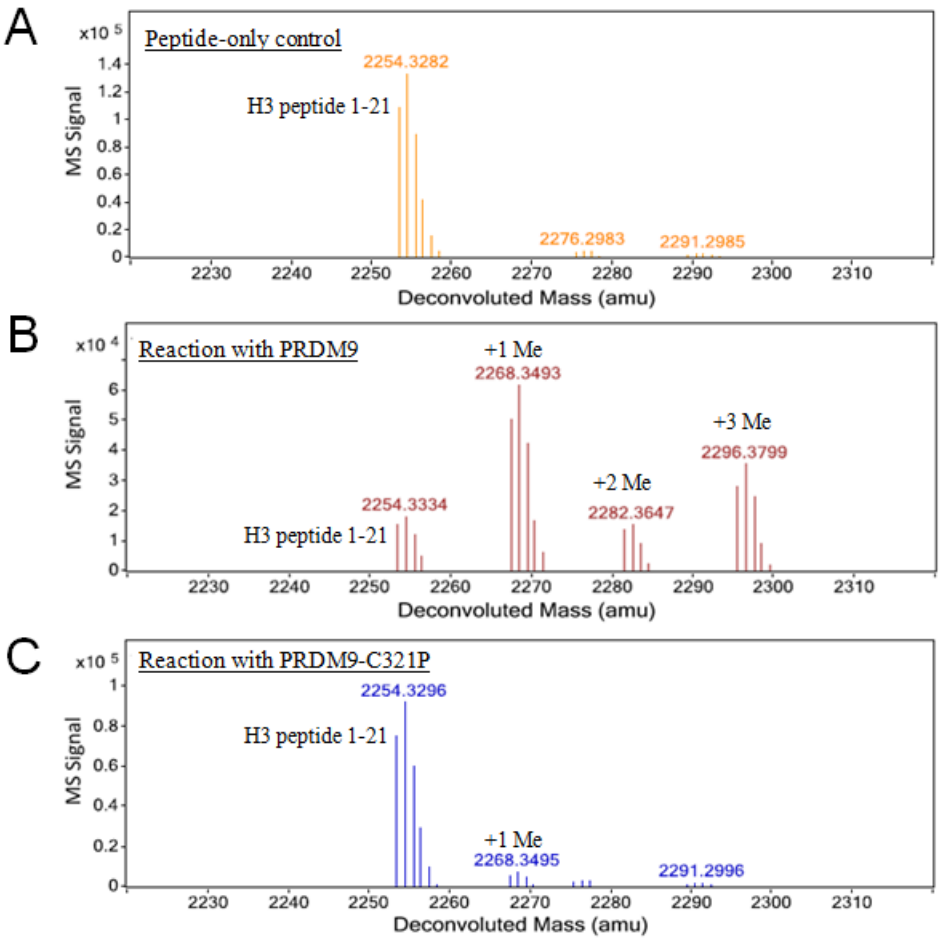
A
Peptide-only control
x10 5
MS Signal
2254.3282
H3 peptide 1-21
2276.2983
2291.2985
Deconvoluted Mass (amu)
B
Reaction with PRDM9
x10 4
+1 Me
2268.3493
+3 Me
2296.3799
+2 Me
2282.3647
2254.3334
H3 peptide 1-21
Deconvoluted Mass (amu)
C
Reaction with PRDM9-C321P
x10 5
2254.3296
H3 peptide 1-21
+1 Me
2268.3495
2291.2996
Deconvoluted Mass (amu)

Figure 8

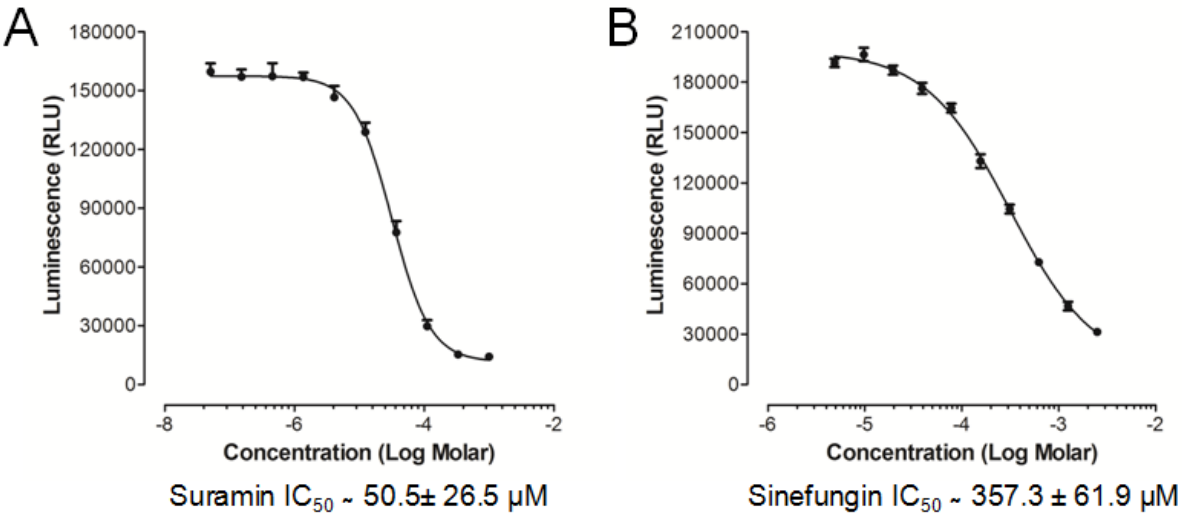
A
Luminescence (RLU)
180000
150000
120000
90000
60000
30000
0
-8
-6
-4
-2
Concentration (Log Molar)
Suramin IC50 ~ 50.5± 26.5 µM
B
Luminescence (RLU)
210000
180000
150000
120000
90000
60000
30000
0
-6
-5
-4
-3
-2
Concentration (Log Molar)
Sinefungin IC50 ~ 357.3 ± 61.9 µM

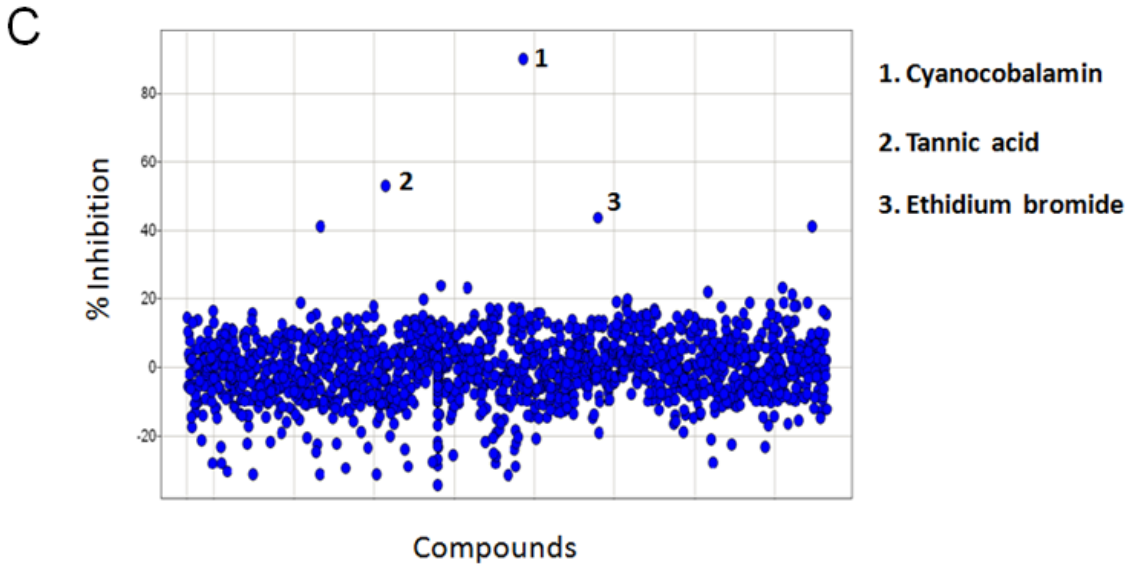
C
% Inhibition
80
60
40
20
0
-20
1
2
3
Compounds
1. Cyanocobalamin
2. Tannic acid
3. Ethidium bromide